Journal of Applied Mathematics and Physics, 2022, 10, 1403-1415
https://www.scirp.org/journal/jamp
ISSN Online: 2327-4379
ISSN Print: 2327-4352

^{181}Ta Nuclei NMR Calculation in Ternary A_3BC_4 Semiconductor

Chen Xu, Chenglong Shi*

College of Science, University of Shanghai for Science and Technology, Shanghai, China
Email: *shichenglong@usst.edu.cn

How to cite this paper: Xu, C. and Shi, C.L. (2022) 181Ta Nuclei NMR Calculation in Ternary A3BC4 Semiconductor. *Journal of Applied Mathematics and Physics*, **10**, 1403-1415.
https://doi.org/10.4236/jamp.2022.105099

Received: March 18, 2022
Accepted: May 6, 2022
Published: May 9, 2022

Copyright © 2022 by author(s) and Scientific Research Publishing Inc.
This work is licensed under the Creative Commons Attribution International License (CC BY 4.0).
http://creativecommons.org/licenses/by/4.0/
Open Access

Abstract

In order to study the electronic structure and the variation of chemical shift of the ^{181}Ta nuclei in ternary A_3BC_4 semiconductor, the first-principles calculations are used by PBE-GGA, BJ, and TB-mBJ functionals. By comparing these three kinds of functionals, the results of TB-mBJ are more in line with the experimental values. The electronic structure calculated by TB-mBJ functional shows that $TaCu_3X_4$ (X = S, Se, Te) are indirect bandgap semiconductors and $TaTl_3X_4$ (X = S, Se) are direct bandgap semiconductors. By decomposing the chemical shifts contributed by the different orbitals, we found that the chemical shifts are related to the electronic structure. In this paper, the variation (up to 2500 ppm) of NMR chemical shift of ^{181}Ta nuclei is related to the d orbital of Ta.

Keywords

NMR, Ternary A_3BC_4 Semiconductor, NMR Chemical Shift, Variation, Bandgap

1. Introduction

Nuclear magnetic resonance (NMR) technology can directly detect the nuclear properties and electronic structure of substances without destroying samples. Its application has been rapidly extended to the fields of physics, chemistry, bioengineering, and so on [1] [2] [3]. The transition energy can be detected by reorienting the nuclear magnetic moment. Due to the existence of electrons outside the nuclei, the induced external magnetic field of the nuclei is shielded by electrons, which is NMR magnetic shielding. In detail, according to Biot-Savart law, the external magnetic field will induce electrons to produce induced current and produce an induced magnetic field, which shields part of the external field. The size of the shield depends on the difference in the electronic structure of the

measured material. NMR spectra provide three kinds of extremely useful information: chemical shift, coupling constant, and integral curve. In this paper, chemical shift is mainly used. However, it is very difficult to accurately determine the chemical shift. The relative numerical representation is adopted, that is, reference material is selected, and the position of the resonance absorption peak of the reference compound is taken as the zero point. The chemical shift values of other absorption peaks are determined according to the distance between the position of these absorption peaks and the zero point [4] [5].

The magnetic shielding calculated by density functional theory is reasonable compared with the experiment. Even, the results of theoretical calculation can provide more information than experiments [6]. For the calculation of solid magnetic shielding, the *ab initio* calculation method is the only feasible method to calculate solid magnetic shielding, because it cannot extract this information directly from the original experimental data like liquid or molecular system. On this basis, a set of *ab initio* calculation methods based on linear response is proposed. Through this method, combined with the all-electron augmented plane-wave (APW) method, we can calculate the NMR tensor in solids and the isotropic shieldings in compounds [7] [8] [9] [10]. Based on this DFT calculation method, some articles on the calculation of solid magnetic shielding appear one after another. Blaha and Laskowski successively studied the magnetic shielding of ^{19}F [11], ^{33}S [12], ^{70}Ga [13], ^{89}Y [14], and so on. Jalali-asadabadi and Nematollahi studied the micro source of solid-state NMR shielding of ^{17}O in titanate of alkaline earth perovskite metals and explored the relationship between atomic and orbital characters of the valence and conduction bands wave functions as well as the ^{17}O NMR shielding [15].

Because transition metal elements have complex electronic structures. Therefore, in this article, we want to discuss the magnetic shielding (shift) of heavy nuclei (^{181}Ta) and the electronic structure of Ta-series compounds in ternary A_3BC_4 semiconductor in detail, to give readers a clearer understanding of the properties of this transition metal semiconductor [16].

In this work, we studied the magnetic shielding of ^{181}Ta nuclei and the electronic structure of $TaCh_3X_4$ (Ch = Cu, Tl; X = S, Se, Te) with different functional (PBE-GGA [17], BJ [18], and TB-mBJ [19]). Firstly, the calculated principle and details of NMR shielding are briefly described. Then, the electronic structure is described by calculating the band structure and density of states. After that, the magnetic shielding of ^{181}Ta nuclei was calculated. We decompose the magnetic shield along the electron orbitals of Ta atom to seek the main source of the variation in the magnetic shielding. Finally, the variation of chemical shifts is analyzed from the perspective of electronic structure.

2. Computational Methods and Details

2.1. Computational Methods

In this study, the application of the all-electron augmented plane wave (APW)

method in different exchange correlations is used by the WIEN2k package [20]. For NMR calculation, applying an external magnetic field $\boldsymbol{B}$ to the given material can induce and generate induced current $\boldsymbol{j}_{ind}$ by extranuclear electrons. In addition, the induced current $\boldsymbol{j}_{ind}$ is directly proportional to the external field. The current generates a non-uniform magnetic field $\boldsymbol{B}_{ind}$, which offsets part of the applied magnetic field, resulting in magnetic shielding. When the applied magnetic field $\boldsymbol{B}$ is small enough, the NMR shielding tensor $\vec{\sigma}(\boldsymbol{R})$ can linearly connect the induced field $\boldsymbol{B}_{ind}$ with the external magnetic field $\boldsymbol{B}$ [4]:

$$\boldsymbol{B}_{ind}(\boldsymbol{R}) = -\vec{\sigma}(\boldsymbol{R})\boldsymbol{B} \tag{1}$$

In practice, the isotropic chemical shift $\vec{\delta}(\boldsymbol{R})$ is the parameter that can be obtained in the experiment. The isotropic chemical shift is the average of the diagonal elements of the chemical shift tensor $\vec{\delta}(\boldsymbol{R})$, that is, $\delta_{iso}(\text{ppm}) = Tr\left[\vec{\delta}(\boldsymbol{R})/3\right]$ [4]. Isotropic chemical shift is the direct result of the experiment, but the isotropic shielding is directly obtained by calculation. Isotropic chemical shift is the difference between the absolute shielding value of the measured material and the absolute shielding value of some reference compounds. Therefore, if you want to calculate the isotropic chemical shift of the measured material, you must calculate the absolute shielding value of the reference compound, i.e. $\delta_{iso}(\boldsymbol{R}) = \sigma_{ref} - \sigma_{iso}(\boldsymbol{R})$ [4]. In this work, the $KTaO_3$ reference is used in ^{181}Ta nuclei [16].

According to Biot-Savart law, the induced magnetic field $\boldsymbol{B}_{ind}$ is obtained by integrating [21]:

$$\boldsymbol{B}_{ind}(\boldsymbol{R}) = \frac{1}{c}\int d\boldsymbol{r}\frac{\boldsymbol{j}_{ind}(\boldsymbol{r})\times(\boldsymbol{R}-\boldsymbol{r})}{|\boldsymbol{R}-\boldsymbol{r}|^3} \tag{2}$$

where c is the speed of light in vacuum, $\boldsymbol{r}$ is the vector about the origin of the crystal coordinate axis system in the real space in a single cell, $\boldsymbol{R}$ is the position vector of the atom in a single cell about the origin of the crystal coordinate axis system, and $\boldsymbol{j}_{ind}(\boldsymbol{r})$ is the induced current density vector.

For non-magnetic materials, only the orbital motions of electrons contribute to $\boldsymbol{j}_{ind}(\boldsymbol{r})$, which can be simplified into the following form [11].

$$\boldsymbol{j}_{ind}(\boldsymbol{r}) = \frac{1}{c}\sum \text{Re}\left[\left\langle \Psi_o^{(0)}\middle|\boldsymbol{J}^0(\boldsymbol{r})\middle|\Psi_o^{(1)}\right\rangle\right] \tag{3}$$

Here, Re represents the real part of the complex number and $\boldsymbol{J}^0(\boldsymbol{r})$ represents the paramagnetic (undisturbed) part of the current operator. $\Psi_o^{(0)}$ is the ground state wave function in the occupied state in the KS equation and $\Psi_o^{(1)}$ is the first-order perturbation wave function in the occupied state. In addition, the occupied first-order perturbation state $\left|\Psi_o^{(1)}\right\rangle$ is related to the empty state $\left|\Psi_e^{(1)}\right\rangle$ above the Fermi surface, which can be connected by Green's function $G(\varepsilon) = \sum_e\left[\left(\left|\Psi_e^{(0)}\right\rangle\left\langle\Psi_e^{(0)}\right|\right)/(\varepsilon-\varepsilon_e)\right]$ [10], that is:

$$\left|\Psi_o^{(1)}\right\rangle >= \sum_e\left|\Psi_e^{(0)}\right\rangle > \frac{\left\langle\Psi_e^{(0)}\middle|\left[r-r'\times\boldsymbol{P}\cdot\boldsymbol{B}\right]\middle|\Psi_o^{(0)}\right\rangle}{\varepsilon_o-\varepsilon_e} \tag{4}$$

In Equation (4) above, $\left|\Psi_e^{(0)}\right\rangle$ is the unperturbed wave function of the empty state, $\boldsymbol{P}$ is the momentum, and the denominator $\varepsilon_o - \varepsilon_e$ is the energy difference between the occupied state and the empty state.

2.2. Computational Details

In this paper, the structural optimization of Ta-series materials is performed in the framework of density functional theory within the VASP [22] [23] (Vienna Ab-initio Simulation Package) program. The cut-off energy is set to 650 eV, the k-points sampling 11 × 11 × 11 is adopted and the energy convergence standard is chosen as $1 \times 10e^{-8}$. These Ta-series materials are divided into two structures, $P\bar{4}3m$ and $I\bar{4}3m$ respectively [16]. The unit cell of $TaCu_3X_4$ consists of eight atoms with a space group which is shown in **Figure 1(a)**. **Figure 1(b)** shows the crystal structure of $TaTl_3X_4$ with a space group of $I\bar{4}3m$.

The optimized lattice parameters are selected and put into the calculation of the WIEN2k program [20]. The electronic structure and NMR properties are calculated by different functionals (PBE-GGA, BJ, and TB-mBJ) in the WIEN2k code. In the WIEN2k program, $R_{MT}K_{max}$ is set to 8, and k-points sampling 10 × 10 × 10 is adopted.

Energy convergence and charge convergence standards are chosen as 0.0001Ry. G_{max} is set to 14 $Ry^{1/2}$. When calculating the NMR magnetic shielding value, to ensure faster and better convergence, NMR-LOs (NMR local orbit) are set to the default value. All other parameters are default values.

3. Results and Discussions

3.1. Electronic Structure

The optimized lattice parameters for Ta-series compounds are calculated by PBE-GGA functional in the solid states. Experimental and theoretical calculated lattice parameters are shown in **Table 1**. The calculated results are in close agreement with experimental lattice parameters. In the WIEN2k program, we calculated the bandgap, band structure, and electronic density of states of Ta-series compounds. As shown in **Table 2**, we calculated the width of the bandgap of

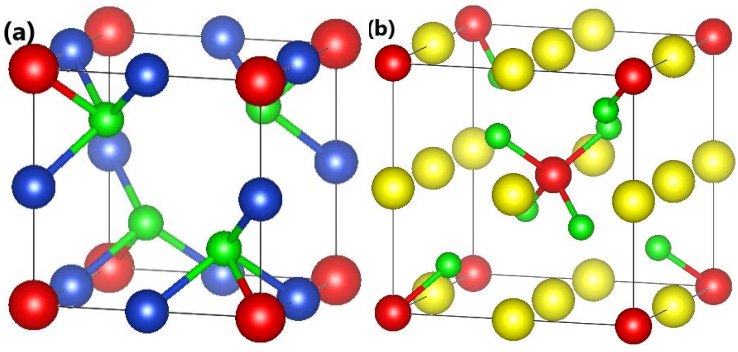

Figure 1. The red, blue and green spheres denote Ta, Cu, X (X = S, Se, Te) in the $P\bar{4}3m$ structure (a). The red, yellow and green spheres denotes Ta, Tl, X (X = S, Se) in the $I\bar{4}3m$ structure (b).

Table 1. The optimized lattice parameters for transition metal semiconductors by using PBE-GGA functional.

Compound	Space group	Lattice Parameters (Å) (Optimization)	Lattice Parameters (Å) (Experiment)
$TaCu_3S_4$	$P\bar{4}3m$	5.573	5.52 [24]
$TaCu_3Se_4$	$P\bar{4}3m$	5.722	5.67 [24]
$TaCu_3Te_4$	$P\bar{4}3m$	6.001	5.928 [25]
$TaTl_3S_4$	$I\bar{4}3m$	7.854	7.671 [26]
$TaTl_3Se_4$	$I\bar{4}3m$	8.076	7.876 [26]
$KTaO_3$	$P\bar{4}3m$	4.037	3.989 [27]

Table 2. A comparison of bandgap values with the experimental data. The bandgap values are in eV.

Compound	E_g^{PBE}	E_g^{BJ}	E_g^{mBJ}	E_g^{exp}
$TaCu_3S_4$	1.935	2.055	2.148	2.7 [28]
$TaCu_3Se_4$	1.616	1.672	1.820	2.35 [28]
$TaCu_3Te_4$	1.162	1.194	1.311	---
$TaTl_3S_4$	2.543	2.770	3.288	---
$TaTl_3Se_4$	2.254	2.461	2.761	---

Ta-series compounds by different functionals (PBE-GGA, BJ, and TB-mBJ). In all compounds, the width of the bandgap calculated by TB-mBJ functional is larger than that calculated by the other two functionals and is closer to the experimental bandgap. In density functional theory, the solution of the Kohn-Sham equation does not consider the excited state of the system, so that the band above the valence band is low, and the position below the valence band is consistent with the experiment, which leads to the underestimate of the bandgap. Generally, the calculated bandgap is 30% to 50% lower than the experiment [17]. This is also the reason why PBE-GGA functional underestimates the size of the bandgap.BJ and TB-mBJ are functionals proposed to improve the underestimation of bandgap in DFT methods. They can more accurately describe the properties near the Fermi level. It can be seen from **Table 2** that the width of the bandgap of both $TaCu_3X_4$ and $TaTl_3X_4$ compounds decreases with the increase of the atomic number of chalcogenide elements.

On the one hand, in order to better describe the electronic structure, we calculated the band structure of Ta-series compounds by using TB-mBJ functional. Since the band structures of compounds with the same crystal structure and similar components are similar, only the band structures of $TaCu_3S_4$ and $TaTl_3S_4$ are given in **Figure 2**.

We can observe from **Figure 2(a)** that the valence band of $TaCu_3S_4$ has two major non-overlapping bands. The band near the Fermi level has a width of about 2.0 eV and is separated by 1 eV from the slightly lower band. The slightly

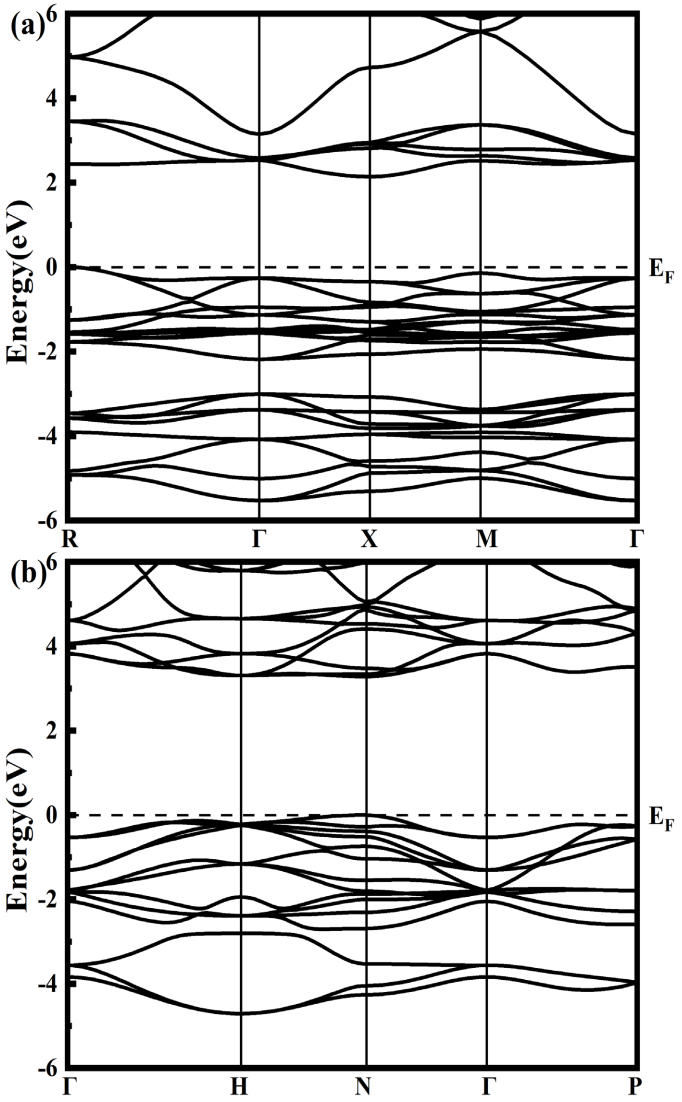

Figure 2. TB-mBJ band structures of $TaCu_3S_4$ (a) and $TaTl_3S_4$ (b), with the VBM set to 0 eV in all cases.

lower band has a width of 2.8 eV. For $TaTl_3S_4$, its valence band consists of two parts that do not overlap. The bandwidth of the lower energy level is about 2 eV, but it is close to the band with slightly higher energy. Moreover, the low-energy band of $TaCu_3S_4$ is denser than that of $TaTl_3S_4$. For the conduction band, there is no separated part of the band of the two compounds. The position and energy density of the conduction band of $TaTl_3S_4$ is higher than that of $TaCu_3S_4$.

The band structures reveal that all of the systems are predicted to possess indirect or direct fundamental bandgaps. For the $TaCu_3S_4$ compound, the VBM and CBM are located at the R and X points, respectively. This means that the $TaCu_3S_4$ compound is a semiconductor with an indirect bandgap. $TaCu_3S_4$ is determined to have the largest bandgap of the $TaCu_3X_4$ compounds, with a direct bandgap of 2.60 eV and an indirect bandgap of 2.10 eV. The experimental bandgap of $TaCu_3S_4$ makes this material (with appropriate doping) an interest-

ing candidate for the p-type transparent conductor. For the $TaTl_3S_4$ compound, a semiconductor with a direct bandgap, both VBM and CBM are located at the N point. Because the electronic transition of semiconductor materials with direct bandgap is easier to occur, $TaTl_3S_4$ has a broad prospect as a luminescent material.

In this paper, five compounds were calculated by PDOS. The valence band top (VBM) is aligned with 0eV (Fermi surface). Since the $TaTl_3Te_4$ compound cannot be synthesized experimentally, the $TaTl_3Te_4$ compound will not be discussed in this article. For $TaCu_3X_4$ compounds, the valence band (VB) has an obvious density of states of Cu 3d band and some Ta 5d band and X mp (X = S, m = 3; X = Se, m = 4; X = Te, m = 5) band. For the conduction band (CB) of $TaCu_3X_4$, there is the density of states of Cu 3d band, Ta 5d band, and some X mp band. For $TaTl_3X_4$ (X = S, Se) compounds, the valence band (VB) has an obvious density of states of X mp band and partial Ta 5d band. Because the outermost electron of Tl is s electron, the density of states of the Tl 6s band appears at the valence band of $TaTl_3X_4$. For $TaTl_3X_4$ compounds, the conduction band (CB) is mainly composed of Ta 5d and X mp bands. It can be seen from **Figure 3** that the 5d orbital of Ta in $TaCh_3X_4$ is an electron unfilled state, so the Ta 5d band

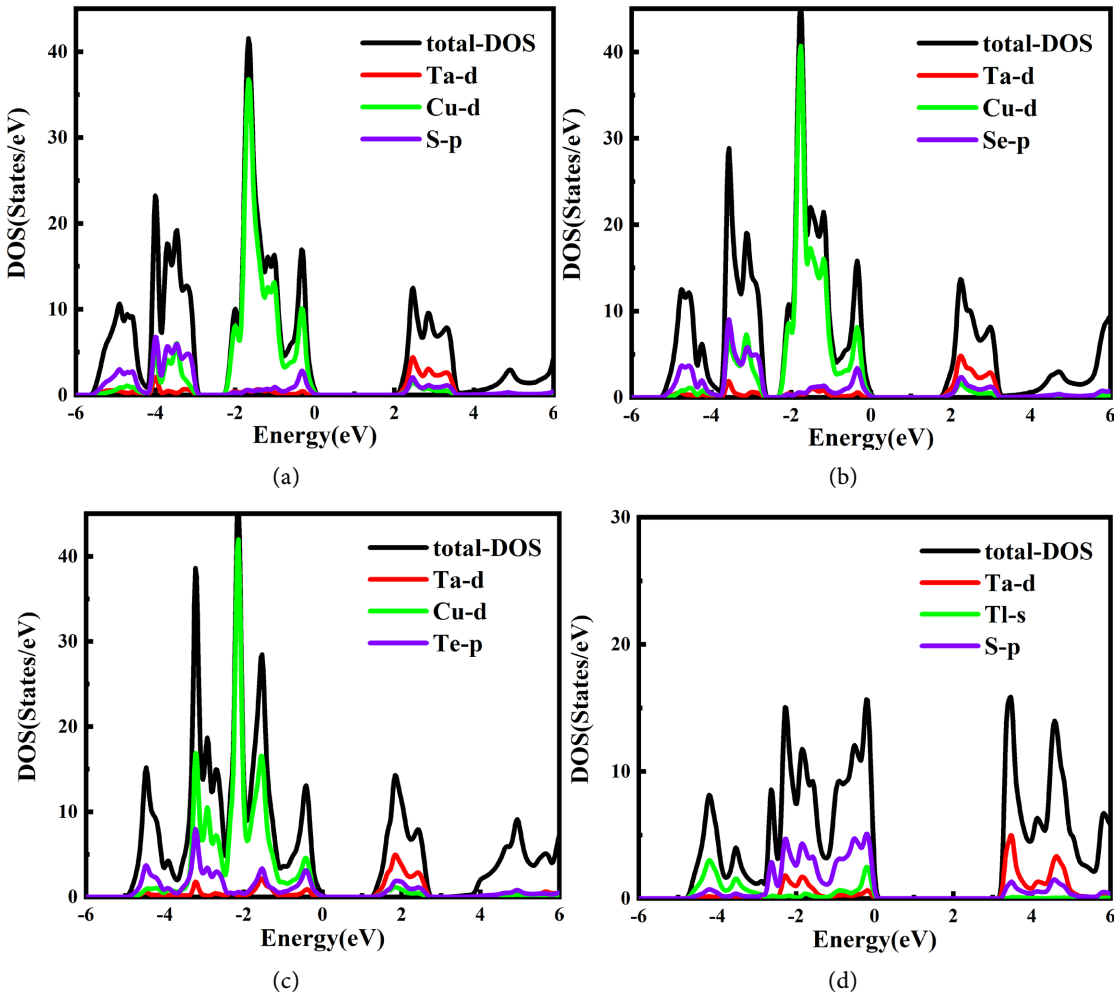

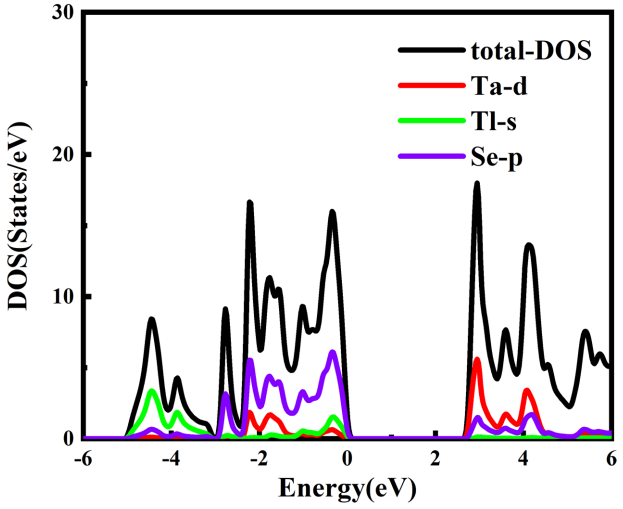

(e)

Figure 3. The calculated density of states for $TaCh_3X_4$. (a) $TaCu_3S_4$; (b) $TaCu_3Se_4$; (c) $TaCu_3Te_4$; (d) $TaTl_3S_4$; (e) $TaTl_3Se_4$.

exists in both the valence band and the conduction band. For Tl 5d, the state is filled with electrons, so the Tl 5d band is located at a relatively deep energy level and does not appear in the valence band. Moreover, we also observed that the bandgap of $TaCu_3X_4$ compounds decreases with the increase of the atomic number of chalcogenide elements (S, Se, Te).

3.2. Chemical Shift

Firstly, we use PBE-GGA, BJ, and TB-mBJ functionals to calculate the magnetic shielding tensors $\ddot{\sigma}(\boldsymbol{R})$ of five compounds. After that, the isotropic shielding σ_{iso} were obtained by $\delta_{iso}(ppm) = Tr\left[\ddot{\sigma}(\boldsymbol{R})/3\right]$. Finally, the calculated isotropic shift δ_{iso} were obtained by $\delta_{iso}(\boldsymbol{R}) = \sigma_{ref} - \sigma_{iso}(\boldsymbol{R})$, as shown in **Table 3**. The final result is the calculated isotropic chemical shifts and the corresponding experimental isotropic chemical shift are linearly fitted by the least square method, as shown in **Figure 4**.

In **Figure 4**, the linear fitting result of PBE-GGA is $\delta_{iso}^{th} = 1.067\delta_{iso}^{exp} - 590.31$, $R^2 = 0.995$, there is a good fitting result. The results of BJ and TB-mBJ have similar trends. If the slope of the above equation is closer to the ideal value 1, the more correct the calculation result is. However, in the calculation, due to the approximation used in exchange functional, wave function basis set and linear response theory, there are some deviations between the calculated values and the experimental values. **Figure 4** clearly shows that different exchange correlation functionals will lead to different slopes and intercepts of linear equations. From the linear fitting results in **Figure 4**, it can be seen that the result of BJ functional is $\delta_{iso}^{th} = 1.067\delta_{iso}^{exp} - 322.03$, $R^2 = 0.975$; the result of TB-mBJ functional is $\delta_{iso}^{th} = 1.022\delta_{iso}^{exp} + 31.29$, $R^2 = 0.992$. In terms of slope, TB-mBJ (1.022) is closer to the ideal slope value than PBE-GGA (1.067) and BJ (1.067). From the perspective of R square, PBE-GGA (0.995) and TB-mBJ (0.992) fit better than BJ

Table 3. Obtained ^{181}Ta σ_{iso} and δ_{iso} values (ppm) by using PBE, BJ and TB-mBJ (mBJ) functionals and compared with the experimental data (δ_{iso}^{exp}). According to $\delta_{iso}(\boldsymbol{R}) = \sigma_{ref} - \sigma_{iso}(\boldsymbol{R})$, δ_{iso}^{th} can be obtained, in which the reference of Ta-series compounds is $KTaO_3$.

Compound	σ_{iso}^{PBE}	σ_{iso}^{BJ}	σ_{iso}^{mBJ}	δ_{iso}^{PBE}	δ_{iso}^{BJ}	δ_{iso}^{mBJ}	δ_{iso}^{exp}
$TaCu_3S_4$	−595.58	−592.62	135.1	2306.4	2600.78	2816.7	2740
$TaCu_3Se_4$	−1795.83	−1846.2	−1020.43	3506.65	3854.36	3972.23	3730
$TaCu_3Te_4$	−3806.1	−3898.29	−2951.62	5516.92	5906.45	5903.42	5720
$TaTl_3S_4$	−1955.02	−1785.34	−1110.76	3665.84	3793.5	4062.56	4070
$TaTl_3Se_4$	−3259.78	−3103.26	−2383.26	4970.6	5111.42	5335.06	5210
$KTaO_3$	1710.82	2008.16	2951.8	0	0	0	---

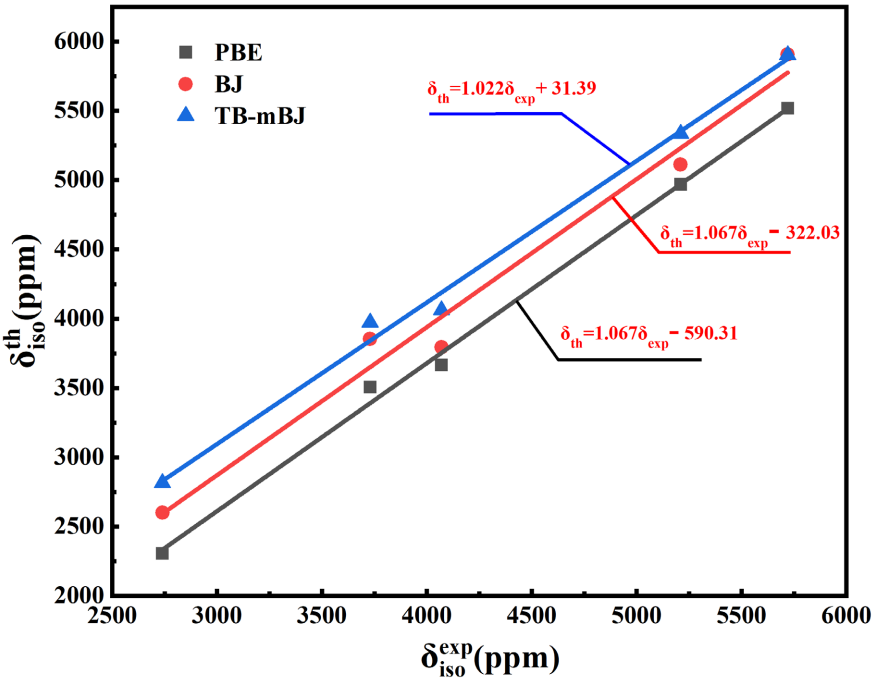

Figure 4. Comparison of the calculated isotropic chemical shifts (δ_{iso}^{th}) by PBE-GGA, BJ and TB-mBJ functionals with experimental isotropic chemical shifts (δ_{iso}^{exp}) for $TaCh_3X_4$ transition-metal semiconductors. The experimental values are taken from ref. [16].

(0.975). In terms of intercept, TB-mBJ (31.29) is much smaller than PBE-GGA (−590.31) and BJ (−322.03). In conclusion, the results of TB-mBJ are more in line with the experimental values. That's because BJ and TB-mBJ (BJ modified by Peter *et al.*) is a functional that precisely optimizes exchange interactions. They can better describe the exchange interaction than PBE-GGA. They can improve the underestimation of the bandgap of PBE-GGA.

Next, we will discuss the NMR shielding σ_{iso} of Ta.

Table 4 shows the decomposed isotropic shielding of Ta in five compounds. The total isotropic shielding amount of Ta (σ_{iso}-total) includes the shielding

Table 4. The partial contributions in total ^{181}Ta NMR isotropic shielding by using TB-mBJ. All values are in ppm. σ-sphere contribution dominates and σ-core contribution is constant in σ-total shielding.

Compound	$TaCu_3S_4$	$TaCu_3Se_4$	$TaCu_3Te_4$	$TaTl_3S_4$	$TaTl_3Se_4$
Total	123.18	−988.48	−2917.61	−1110.99	−2385.16
Core	8786.1	8785.9	8785.5	8785.8	8785.6
Sphere	108.1	−1000.78	−2917.79	−1116.99	−2387.06
interstitial	15.1	12.38	0.18	6.0	1.9
Ta-s	4.56	4.69	3.32	5.27	5.65
Ta-p	−2955.54	−2946.57	−2896.72	−2806.69	−2868.92
Ta-d	−5002.65	−6101.46	−8085.75	−6399.84	−7577.9
Ta-f	−723.59	−742.18	−732.34	−700.84	−729.18

amount of the atomic sphere of (σ_{iso}-sphere) and the shielding amount of interstitial region (σ_{iso}-interstitial) where Ta atomic sphere does not overlap with other atom balls according to APW method. Since the isotropic shielding amount in the interstitial area is about 10 ppm, it nearly has no influence on the total shielding. Therefore, the total isotropic shielding of Ta is almost all contributed by the atomic sphere. As we can see in **Table 4**, total shielding and the shielding of the atomic sphere of Ta almost coincide. Furthermore, the contribution of the atomic sphere (σ_{iso}-sphere) to shielding comes from the contribution of the valence band (σ_{iso}-valence) and core (σ_{iso}-core). It is worth mentioning that the core of Ta is composed of 1s to 4d electrons and the valence band is composed of 5s to 6s electrons. Isotropic shielding contributed by σ_{iso}-core is a constant of 8786 ppm, so the part of core cannot be the reason why the isotropic shielding amount of Ta varies so much with different compounds. Besides, it should be noted that σ_{iso}-valence and total shielding amount vary in the same way. Therefore, we can think that the variation of total isotropic shielding comes from the variation of σ_{iso}-valence.

Next, we decompose the contribution of the orbital to the isotropic shielding according to the s, p, d, f orbital of the valence band. We find that the contribution of the d orbital of Ta to the isotropic shielding is consistent with that of the valence band. This fully shows that the variation of the 5d orbital of Ta is the main reason for the variation of isotropic shielding of these five compounds.

It can be seen from the Equation (3) that the calculation of the induced current of NMR shielding requires the participation of the first-order disturbance wave function, which is obtained through the Equation (4). Equation (4) indicates that the corresponding occupied and unoccupied wave functions are coupled with each other [8]. Therefore, the states of occupied and unoccupied wave functions are bound to affect the results of isotropic shielding. At the same time, we can also see from Equation (4) that its denominator is the difference between the energy of the occupied state and the empty state. In other words, the

bandgap between VBM and CBM is bound to affect the value of NMR isotropic shielding. For example, the bandgap of $TaCu_3S_4$ is 2.148 eV, while the calculated bandgaps of $TaCu_3Se_4$ and $TaCu_3Te_4$ are 1.820 eV and 1.311 eV respectively. Meanwhile, The NMR shielding value of $TaCu_3S_4$ is 123.18 ppm, that of $TaCu_3Se_4$ is −988.48 ppm, and that of $TaCu_3Te_4$ is −2917.61 ppm. This also shows that the variation of the bandgap of these five compounds is related to the variation of isotropic shielding. In fact, the variation of the position of the d orbital of Ta in the valence band and conduction band is the most likely reason for the variation of nuclear magnetic shielding.

4. Conclusions

In this work, the electronic structure and NMR chemical shifts of ^{181}Ta nuclei in ternary A_3BC_4 Semiconductor are calculated. Through the calculation of different functionals (PBE-GGA, BJ, and TB-mBJ), it is found that TB-mBJ functional has the best calculation result for the above properties. According to the band structure, $TaCu_3X_4$ is an indirect bandgap semiconductor and $TaTl_3X_4$ is a direct bandgap semiconductor. PDOS diagram shows that the width of bandgap in Ta-series compounds decreases with the increase of an atomic number of chalcogen elements. Our results also show that the chemical shift parameters are related to the electronic properties. The calculated NMR chemical shifts of ^{181}Ta nuclei show that the variation of chemical shifts is related to the d electron of Ta. More precisely, the position of the d orbital of Ta in the conduction band and valence band leads to the variation of chemical shift. Our work shows that the theoretical calculation can help us acquire the information and interpretation of the NMR experiment more deeply or in more detail.

For first-principle calculations, the comparison of the NMR calculated results with the experimental results can be used to evaluate the accuracy and rationality of first-principle calculations.

Acknowledgements

The authors thank the support of the High Performance Computing Center from University of Shanghai for Science and Technology. This work was supported by the National Natural Science Foundation of China (No. 21905175).

Conflicts of Interest

The authors declare no conflicts of interest regarding the publication of this paper.

References

[1] Hedberg, S.A., Knight, R.J., MacKay, A.L. and Whittall, K.P. (1993) The Use of Nuclear Magnetic Resonance for Studying and Detecting Hydrocarbon Contaminants in Porous Rocks. *Water Resources Research*, **29**, 1163-1170. https://doi.org/10.1029/92WR02540

[2] Dervisoglu, R., Middlemiss, D.S., Blanc, F., Lee, Y.-L., Morgan, D. and Grey, C.P. (2015) Joint Experimental and Computational ^{17}O and ^{1}H Solid State NMR Study of $Ba_2In_2O_4(OH)_2$ Structure and Dynamics. *Chemistry of Materials*, **27**, 3861-3873. https://doi.org/10.1021/acs.chemmater.5b00328

[3] Zhang, Z.T., Dmytriieva, D., Molatta, S., Wosnitza, J., Wang, Y., Helm, M., Zhou, S. and Kuehne, H. (2017) Defect-Induced Magnetism in SiC Probed by Nuclear Magnetic Resonance. *Physical Review B*, **95**, Article ID: 085203. https://doi.org/10.1103/PhysRevB.95.085203

[4] Wasylishen, R., Harris, R.K. and Dm, G. (1996) Encyclopedia of NMR.

[5] Markley, J.L., Bruschweiler, R., Edison, A.S., Eghbalnia, H.R., Powers, R., Raftery, D. and Wishart, D.S. (2017) The Future of NMR-Based Metabolomics. *Current Opinion in Biotechnology*, **43**, 34-40. https://doi.org/10.1016/j.copbio.2016.08.001

[6] Improta, R., Barone, V. and Santoro, F. (2007) *Ab Initio* Calculations of Absorption Spectra of Large Molecules in Solution: Coumarin C153. *Angewandte Chemie International Edition*, **46**, 405-408. https://doi.org/10.1002/anie.200602907

[7] Mauri, F., Pfrommer, B.G. and Louie, S.G. (1996) *Ab Initio* Theory of NMR Chemical Shifts in Solids and Liquids. *Physical Review Letters*, **77**, 5300-5303. https://doi.org/10.1103/PhysRevLett.77.5300

[8] Laskowski, R., Blaha, P. and Tran, F. (2013) Assessment of DFT Functionals with NMR Chemical Shifts. *Physical Review B*, **87**, Article ID: 195130. https://doi.org/10.1103/PhysRevB.87.195130

[9] Bagno, A. and Saielli, G. (2007) Computational NMR Spectroscopy: Reversing the Information Flow. *Theoretical Chemistry Accounts*, **117**, 603-619. https://doi.org/10.1007/s00214-006-0196-z

[10] Laskowski, R. and Blaha, P. (2014) Calculating NMR Chemical Shifts Using the Augmented Plane-Wave Method. *Physical Review B*, **89**, Article ID: 014402. https://doi.org/10.1103/PhysRevB.89.014402

[11] Laskowski, R. and Blaha, P. (2012) Origin of NMR Shielding in Fluorides. *Physical Review B*, **85**, Article ID: 245117. https://doi.org/10.1103/PhysRevB.85.245117

[12] Laskowski, R. and Blaha, P. (2015) Understanding of S-33 NMR Shielding in Inorganic Sulfides and Sulfates. *The Journal of Physical Chemistry C*, **119**, 731-740. https://doi.org/10.1021/jp5095933

[13] Laskowski, R., Khoo, K.H., Haarmann, F. and Blaha, P. (2016) Computational Study of Ga NMR Shielding in Metallic Gallides. *The Journal of Physical Chemistry C*, **121**, 753-760. https://doi.org/10.1021/acs.jpcc.6b11210

[14] Hoeting, C., Eckert, H., Haarmann, F., Winter, F. and Poettgen, R. (2014) Equiatomic Intermetallic Compounds YTX (T = Ni, Ir; X = Si, Ge, Sn, Pb): A Systematic Study by Y-89 Solid State NMR and Sn-119 Mossbauer Spectroscopy. *Dalton Transactions*, **43**, 7860-7867. https://doi.org/10.1039/C4DT00161C

[15] Nematollahi, J. and Jaai-Asadabadi, S. (2018) Microscopic Sources of Solid-State NMR Shielding in Titanate of Alkaline Earth Perovskite Metals. *The Journal of Physical Chemistry C*, **122**, 20589-20601. https://doi.org/10.1021/acs.jpcc.8b05356

[16] Becker, K.D. and Berlage, U. (1983) NMR Chemical Shifts of ^{51}V, ^{93}Nb, ^{181}Ta, and ^{205}Tl in Ternary A_3BC_4 Semiconductors. *Journal of Magnetic Resonance*, **54**, 272-284. https://doi.org/10.1016/0022-2364(83)90049-5

[17] Perdew, J.P., Burke, K. and Ernzerhof, M. (1996) Generalized Gradient Approximation Made Simple. *Physical Review Letters*, **77**, 3865-3868. https://doi.org/10.1103/PhysRevLett.77.3865

[18] Becke, A.D. and Johnson, E.R. (2006) A Simple Effective Potential for Exchange. *The Journal of Chemical Physics*, **124**, Article ID: 221101. https://doi.org/10.1063/1.2213970

[19] Tran, F. and Blaha, P. (2009) Accurate Band Gaps of Semiconductors and Insulators with a Semilocal Exchange-Correlation Potential. *Physical Review Letters*, **102**, Article ID: 226401. https://doi.org/10.1103/PhysRevLett.102.226401

[20] Blaha, P.K.S., Schwarz, K., Madsen, G., Kvasnicka, D. and Luitz, J. (2021) WIEN2k: An Augmented Plane Wave plus Local Orbitals Program for Calculating Crystal Properties, WIEN2k an Augmented Plane Wave plus Local Orbitals Program for Calculating Crystal Properties.

[21] Greiner, W. and Picker, H.S. (1999) Classical Electrodynamics. *Physics Today*, **52**, 78-78. https://doi.org/10.1063/1.882870

[22] Kresse, G. and Furthmuller, J. (1996) Efficiency of *Ab-Initio* Total Energy Calculations for Metals and Semiconductors Using a Plane-Wave Basis Set. *Computational Materials Science* (*Netherlands*), **6**, 15-50. https://doi.org/10.1016/0927-0256(96)00008-0

[23] Kresse, G. and Joubert, D. (1999) From Ultrasoft Pseudopotentials to the Projector Augmented-Wave Method. *Physical Review B*, **59**, 1758-1775. https://doi.org/10.1103/PhysRevB.59.1758

[24] Van Arkel, A.E. and Crevecoeur, C. (1963) Quelques sulfures et séléniures complexes. *Journal of the Less Common Metals*, **5**, 177-180. https://doi.org/10.1016/0022-5088(63)90011-0

[25] Zitter, K., Schmand, J., Wagner, K. and Schllhorn, R. (1984) Isomer Shifts of the 6.2 keV Nuclear Transition of Ta^{181} in Sulvanite Type Ternary Phases Cu_3TaX_4 (X = S,Se,Te). *Materials Research Bulletin*, **19**, 801-805. https://doi.org/10.1016/0025-5408(84)90038-2

[26] Cermak, K. (1985) Ionicity of the Chemical Bond in Tl_3XS_4 Compounds. *Crystal Research and Technology* (*East Germany*), **20**, 619-624. https://doi.org/10.1002/crat.2170200504

[27] Millers, D., Grigorjeva, L., Trepakov, V., Kapphan, S.E. and Boatner, L.A. (2005) X-Ray and Pulsed Electron Beam Excited Luminescence and Optical Absorption in $KTaO_3$ Crystals. *Physica Status Solidi* (*c*), **2**, 200-203. https://doi.org/10.1002/pssc.200460145

[28] Newhouse, P.F., Hersh, P.A., Zakutayev, A., Richard, A., Platt, H., Keszler, D.A. and Tate, J. (2009) Thin Film Preparation and Characterization of Wide Band Gap Cu_3TaQ_4 (Q = S or Se) p-Type Semiconductors. *Thin Solid Films*, **517**, 2473-2476. https://doi.org/10.1016/j.tsf.2008.11.020